Chapter 3

Afterglow Solid-State NMR Spectroscopy

Gili Abramov and Nathaniel J. Traaseth

Abstract

Biomolecular solid-state NMR experiments have traditionally been collected through detection of ^{13}C or ^{15}N nuclei. Since these nuclei have relatively low sensitivity stemming from their smaller gyromagnetic ratios relative to ^{1}H, the time required to collect multi-dimensional datasets serves as a limitation to resonance assignment and structure determination. One improvement in the field has been to employ simultaneous or parallel acquisition techniques with the goal of acquiring more than one dataset at a time and therefore speeding up the overall data collection process. Central to these experiments is the cross-polarization (CP) element, which serves as a way to transfer magnetization between nuclei via magnetic dipolar couplings. In this chapter, we show how residual signal remaining after CP is a polarization source that can be used to acquire additional datasets. The setup of this class of experiments, referred to as *Afterglow* spectroscopy, is described and demonstrated using a membrane protein transporter involved in multidrug resistance.

Key words NMR spectroscopy, Magic-angle-spinning, Solid-state NMR, Sensitivity enhancement, Multiple receiver detection, Membrane proteins, Multidrug resistance

1 Introduction

Solid-state NMR (ssNMR) is a technique used to obtain atomic-scale information on a range of solid-like materials, including amorphous powders and materials, nanoparticles [1], and biomolecular assemblies, such as fibrous aggregates [2], membrane proteins [3–5], viruses [6], and intact cells [7]. One of the major advantages of ssNMR is the ability to probe macromolecules under native-like environments. NMR spectra of solid samples are dominated by anisotropic nuclear spin interactions, which provide insight into conformation and dynamics on a wide range of timescales. These interactions also complicate the spectra by giving broader spectral peaks, thus preventing site-specific resolution. Lowe and Andrew showed that spectra can be simplified by manipulating the angular part of these interactions, $P_2(cos\beta_m)$ [8, 9] where P_2 is the 2nd Legendre polynomial. Spinning the sample faster than the size of the anisotropic interaction at the angle $\beta_m = 54.7^\circ$ relative to the

Ranajeet Ghose (ed.), *Protein NMR: Methods and Protocols*, Methods in Molecular Biology, vol. 1688,
DOI 10.1007/978-1-4939-7386-6_3,

magnetic field led to a remarkable improvement in the observed linewidths. This popular technique is known as magic-angle spinning (MAS).

The ongoing developments in MAS ssNMR methodology continue to break new boundaries, raising the level of complexity of systems amenable to the technique. The introduction of selective isotope labeling schemes [10], ^{1}H detection [11], progresses in structure calculation protocols [12, 13], and access to high field and fast spinning instrumentation allows for the acquisition of high-resolution spectra of bio-macromolecular assemblies [14]. Nevertheless, challenges remain for increasing the sensitivity of detecting low-gyromagnetic nuclei such as ^{15}N and ^{13}C. Efforts toward speeding up data acquisition while maximizing the amount of information gained from an individual data set include the development of nonuniform sampling (NUS) techniques [15], improvements in MAS probe technology [16], and the usage of multiple receivers for simultaneous acquisition techniques [17].

Solution NMR methodology has also focused on improving sensitivity. On this front, it was shown by Kupče et al. that the weak ^{13}C signal at the "tail" of a free induction decay can be transferred to ^{1}H and subsequently detected [18]. This residual or "afterglow" magnetization results in the collection of an additional dataset through the use of a second receiver configured for the ^{1}H channel. The advantage of this approach is that the recycle delay is much longer than the coherence transfer and detection steps and therefore two datasets can be obtained for the total experimental acquisition time of one. The presence of unused residual polarization was also recognized by Pines et al. in ssNMR experiments involving proton enhanced sequences, where multiple CP free induction decay signals were co-added [19]. However, the residual magnetization was largely ignored as pulse sequence development focused on transferred magnetization and not on signals left behind. In 2012, our lab proposed an approach to use residual signal to boost sensitivity by making use of ^{15}N polarization remaining after a frequency-selective cross-polarization period [20]. In this experiment, we were able to detect two multidimensional datasets that correlated ^{15}N with ^{13}CA and ^{15}N with ^{13}CO within proteins by making use of relatively long ^{15}N $T_{1\rho}$ and T_1 relaxation times in motionally restricted samples. The final result gave two complementary heteronuclear correlation datasets without any sensitivity loss in the first experiment and without the need for multiple receivers. It is important to note that a complementary but alternative approach to enhancing polarization was proposed by Gopinath and Veglia, referred to as DUMAS [21]. This technique makes use of simultaneous cross polarization from ^{1}H to both ^{15}N and ^{13}C, a shared acquisition period, and subsequent transfer of magnetization for ^{13}C detection. This powerful method has been combined with the afterglow detection approach to produce up to eight

datasets acquired at the same time [22, 23]. Additional efforts in the field have made use of residual polarization in combination with triple cross-polarization periods [24–26].

In the following sections, we describe the steps required for conducting afterglow N-CA/CO experiments in proteins. Since we cannot ignore the importance of all steps in acquiring afterglow spectra, we detail our step-by-step procedure of experimental setup and demonstrate the methodology on a membrane protein (EmrE) sample involved in multidrug resistance.

2 Materials

2.1 Sample Preparation

Reagents used for the EmrE MAS sample preparation have been described previously [27, 28] and were purchased from different sources as detailed below.

1. $^{13}C_6$-glucose and $^{15}NH_4Cl$, both ~99%. For reverse labeling of specific amino acids, e.g., isoleucine and leucine, unlabeled amino acids were added to the growth medium.
2. *n*-dodecyl-β-D-maltoside (DDM).
3. EmrE was reconstituted into 1,2-dimyristoyl-*sn*-glycero-3-phosphocholine (DMPC).
4. *n*-octyl-β-D-glucoside (OG).
5. Bio-Beads™ SM-2 resin (Bio-Rad Laboratories).
6. Final sample preparation of EmrE involved centrifugation in an Optima™ MAX-XP Ultracentrifuge equipped with TLA-100 and TLA-110 rotors, Beckman Coulter.

2.2 NMR Instrumentation and Data Analysis

1. Samples were packed in 3.2 mm thin-walled zirconia MAS rotors with a volume capacity of ~36 μl. These rotors are capable of spinning up to a maximum rate of ~18 kHz (Agilent or Revolution NMR).
2. All MAS ssNMR spectra were acquired on an Agilent DD2 spectrometer operating at 14.1 T, corresponding to a ^1H Larmor frequency of 600 MHz. All experiments used a bio-MAS probe in triple resonance $^1H/^{13}C/^{15}N$ configuration.
3. For data processing and analysis, NMRPipe [29] and Sparky [30] were used, respectively.

3 Methods

3.1 Adjustment of the Magic Angle

The experimental setup for MAS initiates with the adjustment of the magic angle using natural abundance ^{13}C glycine (*see* **Note 1**). Specifically, the linewidth of the ^{13}CO signal (~178 ppm) from powdered/crystalline glycine is minimized while adjusting the

magic angle (*see* **Note 2**). The carbonyl site has a large chemical shift anisotropy and is therefore sensitive to the rotor angle with respect to the magnetic field. The steps below are carried out after determination of the probe power limitations and the 90° pulse widths using isotopically enriched model compounds (*see* **Note 3**).

1. Place a full rotor of natural abundance glycine into the MAS probe.
2. Find the optimal contact time and power values for ^{1}H to ^{13}C cross-polarization (CP) to ensure sufficient signal-to-noise.
3. Place the spectrometer in "FID scan" mode (Agilent) to display the Fourier transformed 1D ^{13}C spectrum after each transient. This mode is synonymous with the "gs" command on Bruker spectrometers. Ensure no window function is applied prior to the Fourier transform that would broaden the spectrum. Set the zero-fill number to 65,536 or larger to provide sufficient digital resolution ("si" on Bruker; "fn" on Agilent).
4. Adjust the magic angle in an iterative fashion to obtain a linewidth on the ^{13}CO signal of less than ~40 Hz under a spinning frequency of 12.5 kHz. We also typically use 12.5 kHz MAS for protein backbone triple resonance experiments in our 3.2 mm bio-MAS probe [31] at a magnetic field of 14.1 T (600 MHz ^{1}H frequency).

3.2 Shimming and Chemical Shift Referencing

Analogous to solution NMR experiments, it is imperative to have a homogeneous magnetic field to achieve narrow spectral lines. Similarly, it is important to have a reliable chemical shift reference before proceeding with an unknown sample. Both of these steps for MAS are described below.

1. Acquire a 1D ^{13}C CP spectrum of a powder sample of adamantane. Due to the excellent linewidths achievable with adamantane, it is necessary to acquire the FID for ~150 ms and lower the power of the ^{1}H decoupling to a value compatible with the MAS probe.
2. Two signals should be observed in the ^{13}C spectrum. Reference the more deshielded peak to 40.48 ppm [32] (*see* **Note 4**).
3. Using the same adamantane sample, adjust the room temperature shim values to obtain homogeneous and narrow spectral lines. This is done in an iterative manner similar to that described for the glycine sample. A linewidth of 7 Hz or lower can be achieved using the CH_2 peak of adamantane.

3.3 Optimization of CP-MAS on the Protein Sample

Nearly all ssNMR experiments begin with a polarization transfer from the abundant ^{1}H spins to the more insensitive $^{13}C/^{15}N$ spins. Below is the way we optimize CP transfers using a one-dimensional (1D) CP-MAS experiment for ^{1}H to ^{15}N spins.

1. The ^{1}H carrier frequency is set on resonance with the water peak in a direct excitation experiment (4.5–5.0 ppm)
2. RF pulses on the X-channel are first calibrated using model compounds to obtain a full nutation curve for each nucleus. To determine optimal flip angles for the protein sample, a CP sequence followed by a 90° (or 270°) pulse on the X-channel under ^{1}H decoupling is applied. The pulse power is adjusted to give a null signal in this spectrum with the optimal value corresponding to the 90° (or 270°) pulse.
3. A ^{1}H nutation frequency of 100 kHz ($\omega_{1,H}/2\pi$) corresponding to a pulse width of 2.5 μs and a flip angle of 90° is optimized by varying the power level for a 360° pulse (i.e., 10 μs). This is done in a CP experiment by detecting on the X-channel, typically ^{13}C.
4. Optimize CP for ^{1}H to ^{15}N. The power-levels for the ^{1}H-^{15} N CP pulses are adjusted by matching the Hartmann-Hahn condition under spinning $\omega_{1,\,^{1}H} = \omega_{1,\,^{15}N} + n\omega_r$, where ω_1 is the nutation frequency for each of the nuclei and ω_r is the MAS rate. The CP signal is optimized by varying the field strength associated with each channel around the calculated values, while keeping the other channel's power constant.
5. Optimize the CP contact time between ^{1}H and ^{15}N. The time for Hartmann-Hahn spin-lock is arrayed from 0.2 ms to approximately 2 ms. Typically, the optimal value for membrane proteins and crystalline soluble protein samples is 0.75–1.0 ms.

3.4 Detection of Rotary Resonance Conditions

The rotary resonance condition is the matching of a spin-lock nutation field with the rotational rate used for MAS [33]. This match leads to dephasing by means of chemical shift anisotropy (CSA) or dipolar coupling. Since spin-lock periods are used in CP transfers, a major goal of our setup is to avoid the rotary resonance condition to ensure the most efficient transfers from ^{15}N to ^{13}C or vice versa. The pulse sequence we use for detecting the rotary resonance conditions is shown in Fig. 1a [34]. Different than the previous uses of rotary resonance conditions for facilitating magnetization transfer, our goal of using this pulse sequence is to avoid conditions for the double CP transfer steps (*see* Subheading 3.5). Below are steps to find the optimal half-integer conditions of nutation frequencies relative to the spinning rate. The optimization is demonstrated in Fig. 1b, showing an array of 1D experiments applied to the membrane protein EmrE under different ω_1 irradiation powers.

1. Place a [^{13}C, ^{15}N] labeled protein sample into the MAS probe.
2. Find an optimal ^{1}H to ^{15}N CP condition by using the Hartmann-Hahn matching condition under MAS (*see* Subheading 3.3).

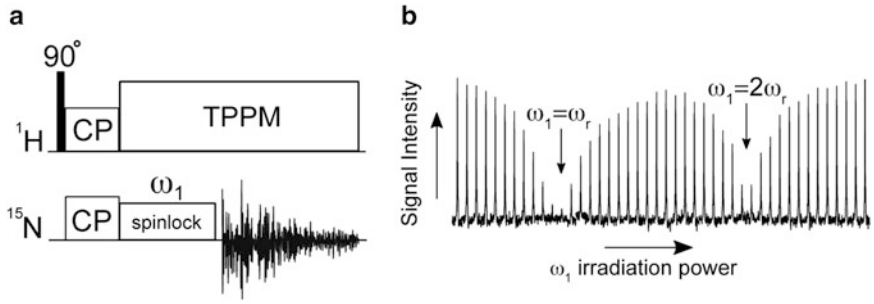

Fig. 1 Empirical detection of rotary resonance conditions. (**a**) Pulse scheme of the rotary resonance experiment. (**b**) Variation of the ω_1 amplitude around the two matching conditions ($\omega_1 = n\omega_r$, $n = 1$ or 2). The experiment is demonstrated on the ^{15}N amide signal in [U-^{15} N,^{13}C] labeled EmrE protein, using a 2 ms pulse length on ^{15}N

3. Find conditions that meet the rotary resonance condition: $\omega_1 = n\omega_r$ ($n = 1, 2$). Set up an array where the continuous-wave (CW) ^{15}N RF powers are adjusted, as shown in Fig. 1b. This is a $T_{1\rho}$ experiment that should be applied with a ^{15}N spin-lock of 2–5 ms. The lowest signals shown in Fig. 1b correspond to the rotary resonance conditions, while the maximum signal intensities following the spin-lock are ideal conditions (i.e., half-integer) to be used in double CP experiments described in subsequent sections.

3.5 Optimization of the DCP Transfers ^{15}N-^{13}CA/^{13}CO

Most heteronuclear correlations in multi-dimensional spectra of solid-like biological samples originate from ^{15}N-^{13}C dipolar couplings. These contacts are usually obtained by selective transfer techniques, correlating the ^{15}N chemical shift with its neighboring ^{13}CA and ^{13}CO chemical shifts. Selective N–CA *or* N–CO transfers are achieved by double cross polarization (DCP or "SPECIFIC CP") Schemes [35, 36]. To achieve a band selective transfer, the irradiation conditions for both rare spin channels are optimized in a 1D N–CA/CO experiment as follows:

1. For band selective excitation, set the carrier frequency to the desired spectral region, i.e., CA at ~55 ppm or CO at ~178 ppm.
2. To achieve magnetization transfer between ^{15}N and ^{13}C nuclei, we initially set the RF amplitudes to $1.5\omega_r$ and $2.5\omega_r$ for ^{13}CA and ^{15}N channels, and $3.5\omega_r$ and $2.5\omega_r$ for ^{13}CO and ^{15}N channels, respectively (*see* **Note 5**). The DCP condition for ^{15}N is set using the steps outlined in Subheading 3.4, which is an empirical way to avoid rotary resonance conditions. In the case for ^{13}CO, it is preferable to apply a higher power on the ^{13}C channel due to the weaker ^{1}H-^{13}CO dipolar couplings than those present for ^{13}CA [37, 38].

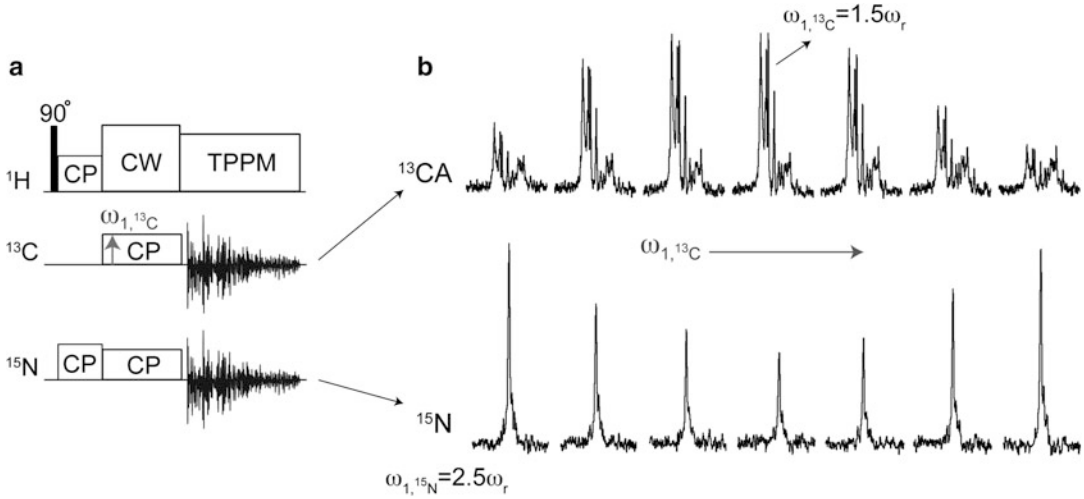

Fig. 2 Optimization of DCP ^{15}N to ^{13}CA transfer. (**a**) Pulse sequence used for optimizing the DCP from ^{15}N to ^{13}CA. The multiple receiver detection is not required for the setup but used to emphasize the reduction in ^{15}N signal as the ^{13}CA signal builds up. **(b)** The ^{13}C amplitude is varied around the calculated 1.5ω_r condition. *Top*: ^{13}CA signal variation. *Bottom*: ^{15}N signal as the ^{13}CA RF amplitude is varied

3. Once the initial power level for the DCP condition is calculated for ^{13}C, a careful optimization of the RF amplitude on the ^{13}C channel is carried out using a pulse sequence similar to that shown in Fig. 2a. An example for the optimization of the DCP condition in N–CA experiment is shown in Fig. 2b. In this experiment we have carried out acquisitions on both ^{15}N and ^{13}C in a simultaneous fashion using multiple receivers. This is not required for the set-up, but is used to emphasize that optimal transfer to ^{13}C gives the highest signal-to-noise in 1D datasets and the lowest signal intensities remaining on ^{15}N. Notably, even after finding optimal transfer conditions, residual polarization remains on ^{15}N and is the basis for our afterglow experiments (*see* Subheading 3.7). Lastly, when optimizing selective transfers, it is important to obtain the highest possible signal intensities while ensuring selectivity to either ^{13}CA or ^{13}CO.
4. DCP contact time optimization. The time for which the ^{15}N and ^{13}C simultaneous pulses are applied is adjusted from 2 to 6 ms. We normally find optimal values from 4 to 5.5 ms.

3.6 Optimization of the Mixing Period for Optional N-CX Correlations

It is often desirable to establish correlations between ^{15}N and side-chain ^{13}C atoms. These contacts are obtained by applying a mixing period prior to the detection of the FID acquisition. Magnetization can be transferred efficiently from CA/CO to nearby ^{13}C atoms by utilizing the dense proton network, commonly present in protein samples (proton-driven spin-diffusion, PDSD). The transfer efficiencies can be further improved upon application of a CW irradiation to

^{1}H during the mixing time at a frequency match corresponding to $\omega_{1,H} = n\omega_r$ ($n = 1$ *or* 2) (i.e., the DARR/RAD condition [39, 40]). The DARR condition is optimized by varying the CW ^{1}H power around the $n = 1$ or $n = 2$ DARR values in a 1D ^{13}C CP-MAS experiment to ensure efficient transfers among ^{13}C spins. The optimal conditions correspond to better dipolar recoupling characterized by a minimum signal in the array for ^{13}C nuclei receiving magnetization from ^{15}N (i.e., CA or CO).

3.7 Acquisition of Afterglow ^{15}N-^{13}CA/^{15}N-^{13}CO

The afterglow pulse scheme is shown in Fig. 3 and involves two acquisition periods for the simultaneous detection of 2D N–CA (first acquisition) and 2D N–CO (second acquisition, using residual ^{15}N polarization). To achieve selective CA- or CO-only detection, the DARR mixing period is set to zero. The optimal pulse widths/powers and initial CP and DCP conditions are found as described above, and are implemented into the current experiment. The two datasets are separated by a ^{13}C transverse magnetization dephasing period, followed by a 90° pulse on the ^{15}N channel to store the residual ^{15}N magnetization along the z-axis after the first DCP. The N–CO experiment is then initiated by a DCP selective transfer from the remaining ^{15}N signal to ^{13}CO spins. The latter dataset is effectively "free of charge" and its sensitivity can be evaluated by comparing to the usual N-CA/CO datasets.

The experimental parameters for the afterglow experiment are essentially the optimized parameters described in Subheadings 3.3–3.6. Nevertheless, in practice, it is necessary to re-optimize the power levels on ^{13}CO in the afterglow experiment in order to achieve maximal signal-to-noise. Figure 4 shows the comparison of

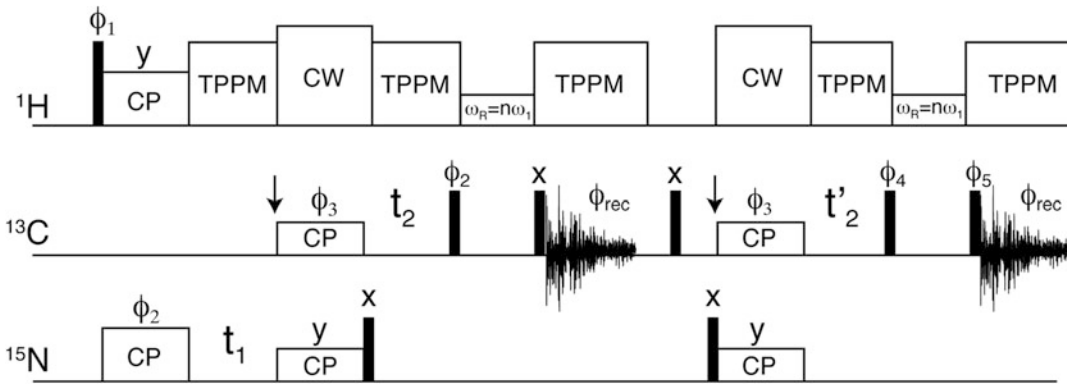

Fig. 3 Afterglow pulse sequence for acquiring N–CA/N–CO in a sequential fashion. The narrow rectangles correspond to 90° pulses. The left and right arrows within the ^{13}C channel signify the offset positioned on the ^{13}CA and ^{13}CO regions, respectively. Phases are: $\phi_1 = (x, -x)$, $\phi_2 = (y)$, $\phi_3 = (x, x, y, y)$, $\phi_4 = (-y, -y, -x, -x)$, $\phi_5 = (y, y, -x, -x)$, and $\phi_{rec} = (x, -x, -y, y)$. To obtain phase-sensitive data in t_1 and t_2, ϕ_2 and ϕ_3 were phase-shifted by 90°, respectively. After the first FID acquisition, a 5 ms time was allowed to dephase residual ^{13}C magnetization. (Reprinted with permission from [20]. © 2012 American Chemical Society)

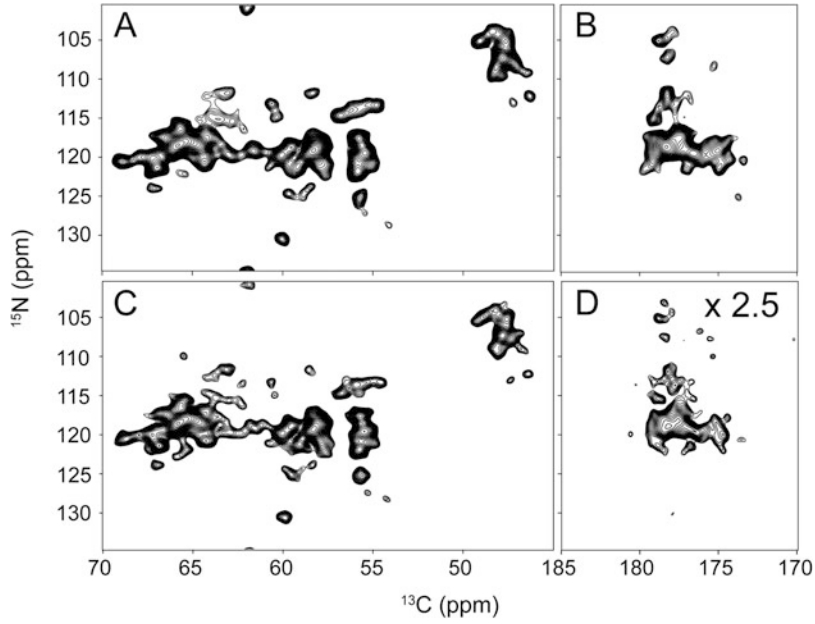

Fig. 4 Two-dimensional N–CA (**a**, **c**) and N–CO (**b**, **d**) spectra of uniformly ^{15}N and ^{13}C enriched EmrE. Standard N–CA spectrum (**a**) and N–CA as part of the Afterglow scheme (**c**) gave similar signal-to-noise ratios. Standard N–CO (**b**) and Afterglow N–CO (**d**). The latter is multiplied by 2.5 to compare with the standard experiment. Overall, the Afterglow N–CO results in about 30–35% of the signal of the standard N–CO for [U-^{15} N,^{13}C] labeled samples

standard 2D N–CA/CO with the afterglow experiments collected using the four transmembrane domain protein EmrE in DMPC liposomes.

3.8 Benefit of Spectroscopic Filtering with the Use of Afterglow

NMR is an inherently insensitive technique. Acquisition of multidimensional datasets on low gyromagnetic ratio nuclei presents additional challenges that further increase experimental times for protein samples. Thus, the development of parallel acquisition techniques is of high importance in the field. The afterglow scheme is advantageous for the following reasons:

1. It utilizes residual magnetization produced in the course of a "regular" heteronuclear experiment to obtain another dataset that can be complementary for the assignment process of biomolecules.
2. It is a simple scheme that does not require specific hardware modifications, and can be applied in any conventional ssNMR spectrometer.
3. The afterglow sequence acquires two ^{15}N-^{13}C correlation spectra using a single recycle delay, which effectively maintains the same overall experimental time with respect to standard datasets.

We have described how Afterglow magnetization from residual ^{15}N signal at the end of a DCP period in 2D N–CA is utilized to obtain a high-quality 2D N–CO spectrum. The comparison between the standard N–CA/CO and the Afterglow N–CA/CO (Fig. 4) acquired on a membrane protein shows the applicability of the methodology to a complex biological system. The signal-to-noise in the afterglow N–CO experiment can be dramatically improved with the usage of sparse isotope labeling schemes (e.g., 1,3-^{13}C or 2-^{13}C glycerol labeling) due to the effect of spin-dilution [41]. Lastly, it is also possible to use the afterglow technique in combination with reverse labeling to further seed chemical shift assignments of congested spectra [41] and for measuring spin relaxation times [42].

4 Notes

1. It is also common to use potassium bromide (KBr) while detecting the ^{79}Br signal.
2. The state of glycine crystallinity or polycrystallinity can impact the observed linewidth.
3. Throughout the set-up process it is important to emphasize that high-power probe tuning is performed to minimize the ratio of forward and reflected powers using an oscilloscope. The ratio between the forward/reflected powers should be equal to or larger than ~25/1.
4. The ^{15}N chemical shift spectrum can be indirectly referenced from the ^{13}C adamantane by using the ratio of reference frequencies for ^{15}N and ^{13}C (0.402979954), as previously described [43, 44].
5. To match up the DCP condition, RF amplitudes must be applied that both satisfy the Hartmann-Hahn condition and avoid the rotary resonance condition. Therefore, frequency irradiation of half-integer multiples of the spinning rate is usually applied to the rare-spins channels, while a high-power CW pulse is simultaneously applied to the abundant ^{1}H channel.

Acknowledgments

This work was supported by NSF (MCB1506420) and NIH (R01AI108889).

References

1. Gutmann T, Grünberg A, Rothermel N et al (2013) Solid-state NMR concepts for the investigation of supported transition metal catalysts and nanoparticles. Solid State Nucl Magn Reson 55:1–11
2. Heise H, Hoyer W, Becker S et al (2005) Molecular-level secondary structure, polymorphism, and dynamics of full-length a-synuclein fibrils studied by solid-state NMR. Proc Natl Acad Sci USA 102:15871–15876
3. Opella SJ, Marassi FM (2004) Structure determination of membrane proteins by NMR spectroscopy. Chem Rev 104:3587–3606
4. Hong M, Zhang Y, Hu F (2012) Membrane protein structure and dynamics from NMR spectroscopy. Annu Rev Phys Chem 63:1–24
5. Wylie BJ, Do HQ, Borcik CG, Hardy EP (2016) Advances in solid-state NMR of membrane proteins. Mol Phys 114(24):3598–3609
6. Quinn CM, Lu M, Suiter CL et al (2015) Magic angle spinning NMR of viruses. Prog Nucl Magn Reson Spectrosc 86:21–40
7. Takahashi H, Ayala I, Bardet M et al (2013) Solid-state NMR on bacterial cells: selective cell wall signal enhancement and resolution improvement using dynamic nuclear polarization. J Am Chem Soc 135:5105–5110
8. Andrew ER, Bradbury A, Eades GR (1958) Nuclear magnetic resonance spectra from a crystal rotated at high speed. Nature 182:1659–1659
9. Lowe IJ (1959) Free induction decays of rotating solids. Phys Rev Lett 2:285–287
10. Hong M (1999) Determination of multiple φ-torsion angles in proteins by selective and extensive ^{13}C labeling and two-dimensional solid-state NMR. J Magn Reson 139:389–401
11. Zhou DH, Shah G, Cormos M et al (2007) Proton-detected solid-state NMR spectroscopy of fully protonated proteins at 40 kHz magic-angle spinning. J Am Chem Soc 129:11791–11801
12. Loquet A, Sgourakis NG, Gupta R et al (2012) Atomic model of the type III secretion system needle. Nature 486:276–279
13. Wang S, Munro RA, Shi L et al (2013) Solid-state NMR spectroscopy structure determination of a lipid-embedded heptahelical membrane protein. Nat Methods 10:1007–1012
14. Bertini I, Emsley L, Lelli M et al (2010) Ultrafast MAS solid-state NMR permits extensive ^{13}C and ^{1}H detection in paramagnetic metalloproteins. J Am Chem Soc 132:5558–5559
15. Paramasivam S, Suiter CL, Hou G et al (2012) Enhanced sensitivity by nonuniform sampling enables multidimensional MAS NMR spectroscopy of protein assemblies. J Phys Chem B 116:7416–7427
16. McNeill SA, Gor'kov PL, Shetty K et al (2009) A low-E magic angle spinning probe for biological solid state NMR at 750 MHz. J Magn Reson 197:135–144
17. Kupče Ē (2011) NMR with multiple receivers. In: Mod. NMR Methodol. Springer, Berlin, pp 71–96
18. Kupče E, Kay LE, Freeman R (2010) Detecting the "afterglow" of ^{13}C NMR in proteins using multiple receivers. J Am Chem Soc 132:18008–18011
19. Pines A, Gibby MG, Waugh JS (1973) Proton-enhanced NMR of dilute spins in solids. J Chem Phys 59:569–590
20. Banigan JR, Traaseth NJ (2012) Utilizing afterglow magnetization from cross-polarization magic-angle-spinning solid-state NMR spectroscopy to obtain simultaneous Heteronuclear multidimensional spectra. J Phys Chem B 116:7138–7144
21. Gopinath T, Veglia G (2012) Dual acquisition magic-angle spinning solid-state NMR-spectroscopy: simultaneous acquisition of multidimensional spectra of biomacromolecules. Angew Chem Int Ed Engl 51:2731–2735
22. Gopinath T, Veglia G (2013) Orphan spin operators enable the acquisition of multiple 2D and 3D magic angle spinning solid-state NMR spectra. J Chem Phys 138:184201
23. Gopinath T, Veglia G (2016) Multiple acquisitions via sequential transfer of orphan spin polarization (MAeSTOSO): how far can we push residual spin polarization in solid-state NMR? J Magn Reson 267:1–8
24. Mote KR, Gopinath T, Veglia G (2013) Determination of structural topology of a membrane protein in lipid bilayers using polarization optimized experiments (POE) for static and MAS solid state NMR spectroscopy. J Biomol NMR 57:91–102
25. Das BB, Opella SJ (2016) Simultaneous cross polarization to ^{13}C and ^{15}N with ^{1}H detection at 60kHz MAS solid-state NMR. J Magn Reson 262:20–26
26. Akbey Ü, Camponeschi F, van Rossum B-J, Oschkinat H (2011) Triple resonance cross-polarization for more sensitive ^{13}C MAS NMR spectroscopy of Deuterated proteins. ChemPhysChem 12:2092–2096

27. Banigan JR, Gayen A, Cho M-K, Traaseth NJ (2015) A structured loop modulates coupling between the substrate-binding and dimerization domains in the multidrug resistance transporter EmrE. J Biol Chem 290:805–814
28. Banigan JR, Gayen A, Traaseth NJ (2015) Correlating lipid bilayer fluidity with sensitivity and resolution of polytopic membrane protein spectra by solid-state NMR spectroscopy. Biochim Biophys Acta 1848:334–341
29. Delaglio F, Grzesiek S, Vuister GW et al (1995) NMRPipe: a multidimensional spectral processing system based on UNIX pipes. J Biomol NMR 6:277–293
30. Goddard TD, Kneller DG SPARKY 3. https://www.cgl.ucsf.edu/home/sparky/
31. Stringer JA, Bronnimann CE, Mullen CG et al (2005) Reduction of RF-induced sample heating with a scroll coil resonator structure for solid-state NMR probes. J Magn Reson 173:40–48
32. Morcombe CR, Zilm KW (2003) Chemical shift referencing in MAS solid state NMR. J Magn Reson 162:479–486
33. Oas TG, Griffin RG, Levitt MH (1988) Rotary resonance recoupling of dipolar interactions in solid-state nuclear magnetic resonance spectroscopy. J Chem Phys 89:692–695
34. Gan Z (2006) Rotary resonance echo double resonance for measuring heteronuclear dipolar coupling under MAS. J Magn Reson 183:235–241
35. Schaefer J, McKay R, Stejskal E (1979) Double-cross-polarization NMR of solids. Academic Press, New York
36. Baldus M, Petkova AT, Herzfeld J, Griffin RG (1998) Cross polarization in the tilted frame: assignment and spectral simplification in heteronuclear spin systems. Mol Phys 95:1197–1207
37. Ishii Y, Ashida J, Terao T (1995) ^{13}C-^{1}H dipolar recoupling dynamics in ^{13}C multiple-pulse solid-state NMR. Chem Phys Lett 246:439–445
38. Franks WT, Kloepper KD, Wylie BJ, Rienstra CM (2007) Four-dimensional heteronuclear correlation experiments for chemical shift assignment of solid proteins. J Biomol NMR 39:107–131
39. Takegoshi K, Nakamura S, Terao T (2001) ^{13}C–^{1}H dipolar-assisted rotational resonance in magic-angle spinning NMR. Chem Phys Lett 344:631–637
40. Morcombe CR, Gaponenko V, Byrd RA, Zilm KW (2004) Diluting abundant spins by isotope edited radio frequency field assisted diffusion. J Am Chem Soc 126:7196–7197
41. Banigan JR, Gayen A, Traaseth NJ (2013) Combination of ^{15}N reverse labeling and afterglow spectroscopy for assigning membrane protein spectra by magic-angle-spinning solid-state NMR: application to the multidrug resistance protein EmrE. J Biomol NMR 55:391–399
42. Good D, Pham C, Jagas J et al. (2017) Solid-state NMR provides evidence for small-amplitude slow domain motions in a multispanning transmembrane α-Helical Protein. J Am Chem Soc 139(27):9246–9258.
43. Harris RK, Becker ED, Cabral de Menezes SM et al (2002) NMR nomenclature: nuclear spin properties and conventions for chemical shifts. IUPAC recommendations 2001. International Union of Pure and Applied Chemistry. Physical chemistry division. Commission on molecular structure and spectroscopy. Magn Reson Chem 40:489–505
44. Siemer AB, Ritter C, Steinmetz MO et al (2006) ^{13}C, ^{15}N resonance assignment of parts of the HET-s prion protein in its amyloid form. J Biomol NMR 34:75–87